10CUEE CONFERENCE PROCEEDINGS
10th International Conference on Urban Earthquake Engineering
March 1-2, 2013, Tokyo Institute of Technology, Tokyo, Japan

USE OF AIRBORNE OPTICAL AND THERMAL IMAGERY FOR THE DETECTION OF BUILDING DAMAGE DUE TO THE 2012 TSUKUBA TORNADO

Fumio Yamazaki[1], Daiki Hanada[2] and Kentaro Suzuki[2]

1) Professor, Department of Urban Environment System, Chiba University, Japan
2) Graduate student, Department of Urban Environment System, Chiba University, Japan
fumio.yamazaki@faculty.chiba-u.jp, d.hanada@chiba-u.jp, z9t0222@students.chiba-u.jp

Abstract: On May 6, 2012, a strong tornado attacked Tsukuba City, Ibaraki Prefecture, Japan. It has caused heavy property losses in a concentrated area. An early detection of building damage is very important for quick response after an occurrence of natural disasters. Aerial visible images are widely used to detect building damage because they can cover a wide area quickly with very high spatial resolution. However, these images cannot be taken without sunlight, which could generate a "blank time" if a disaster occurs in the nighttime. On the other hand, aerial thermal-infrared images can be taken both in the daytime and nighttime without depending on sunlight although it has an inferior spatial resolution compared with aerial visible images. It is considered to be possible to detect building damage from the temperature distribution of an urban surface. In this study, detection of building damage and debris is carried out from aerial thermal-infrared images taken over Tsukuba City on May 8, 2012, both at daytime and nighttime. Spatial characteristics of temperature distribution, such as non-uniformity, are considered to grasp building damage and debris.

1. INTRODUCTION

On May 6, 2012, three powerful tornados were generated in Tochigi and Ibaraki Prefectures, Japan, almost at the same time. These tornados caused severe property losses and some casualties although in narrow areas, such as Tsukuba City. This event was considered to be a good case to test the capability of airborne remote sensing in damage detection, especially using visible and thermal infrared imagery (van Aardt *et al.*, 2011).

Remote sensing is widely used especially for the sites where the access from the ground is limited and the damage distribution covers wide areas (Rathje and Adams, 2008; Eguchi *et al.*, 2008; Dell' Acqua and Gamba, 2012). Various platforms and sensors have been developed recently for satellite remote sensing and its spatial resolution has been improved significantly (Joyce *et al.*, 2009), Airborne remote sensing, however, still has advantages over satellite remote sensing in spatial resolution, immediacy and applicability in cloudy conditions by flying under high-altitude clouds.

Damage detection using visible imagery is simple and common. However, visible imagery cannot be taken in the nighttime, and thus "blank time" may occur in emergency response after a disaster strikes. On the other hand, thermal infrared (TIR) imagery can be taken both in the daytime and nighttime without depending on sunlight. Yamazaki *et al.* (2009) confirmed that clear edges of buildings, roads, and vegetation can be extracted from aerial TIR images of urban areas. Hanada and Yamazaki (2012) recently used ASTER's TIR images for grasping flooded areas by tsunamis caused by the March 11, 2011 Tohoku, Japan earthquake. Satellite TIR imagery, however, has low spatial resolution, e.g. 90 m for ASTER and 60 m for Landsat-7. Hence, its application to small-scale damage is difficult. However, airborne TIR imagery has much higher spatial-resolution, say order of 2 to 3 m, and hence, it can be used for damage detection of individual buildings, especially at nighttime when visible sensors cannot be used.

In this study, we acquired visible and TIR images from a helicopter two days after the tornado in Tsukuba City. The TIR images taken at daytime and nighttime were compared with the visible image at daytime. Visual damage inspection was first carried out by the authors using the daytime visible image for a hard-hit area of the city. The TIR images were then compared with the result of the damage inspection. The temperature distribution from the TIR images was further investigated by employing building footprints from the visible image and GIS. The temperature distribution within a footprint was compared with the damage grade of the building and the capability of aerial TIR images in damage detection was studied.

2. THE MAY 6, 2012 TORNADO IN TSUKUBA

A strong tornado was generated in Joso City, Ibaraki Prefecture, on May 6, 2012 at 12:35. It caused significant damages along its path with 17 km in length and 500 m in width until its end at Tsukuba City (**Figure 1**). The moving speed of the tornado was about 60 km/h (passing 17 km in 18 min) based on the analysis of meteorological Radar by Japan Meteorological Agency (JMA, 2012). JMA judged the Fujita scale of the tornado as F2 (the average wind speed of 50-69 m/s in 7 s) based on their field survey after it passed

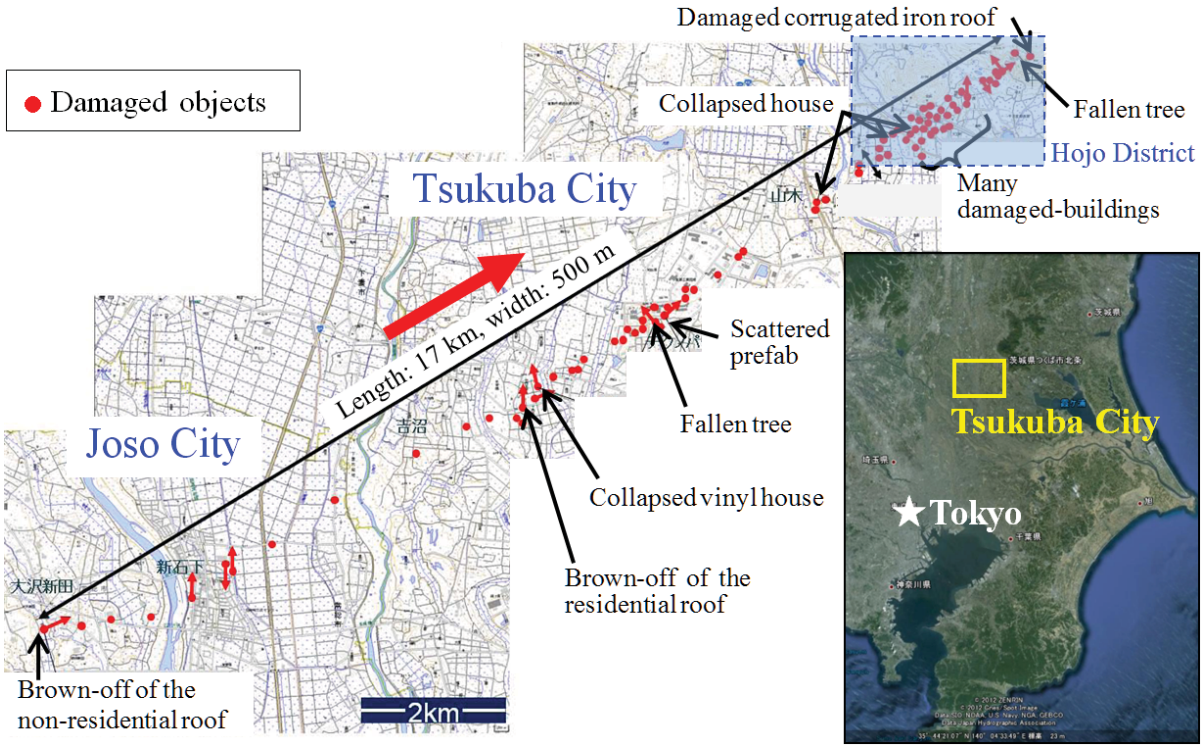

Figure 1 Detail map of the tornado's path and resultant damages, modified from JMA (2012).

by. However, it was changed to F3 (the average wind speed of 70-92 m/s in 5 s) in June 8, 2012 because the resultant damages were found to be so severe; for example, one wood-frame house was overturned upside-down with its concrete base.

This event is ranked as one of the strongest and most damaging tornados in Japan. By this tornado, one person was killed and 37 people were injured as of May 9, 2012, and 1093 buildings were damaged as of August 31, 2012 only in Tsukuba (Tsukuba City, 2012). In the recent years, the number of strong tornados is increasing in Japan, probably due to the climate change. Prediction of the occurrence time and location of a tornado is still very difficult because its time-span is short and its affecting area is small. However, enhancement of tornado prediction, its early warning and rapid response are strongly desired to reduce human casualties due to tornados.

We conducted a field survey of Hojo district, Tsukuba City, to obtain ground truth data from 14:00 to 16:00 on May 8, 2012, almost at the same time of our daytime's aerial image acquisition. Typical damages by the tornado were blown-off of building roofs, broken windows, and falling-down of trees and electric poles. Since these types of damages, other than the damage to building walls, can generally be observed from vertical imagery, we thought this is a good opportunity to test the capability of aerial TIR imagery for building damage assessment as well as that of optical imagery. We surveyed the hard-hit area and took ground photos of severely damaged buildings with their GPS location data.

The route of our field survey in Hojo district on May 8, 2012 was shown by the blue line in **Figure 2a**. We walked around the hard-hit area with digital cameras and hand-held GPSs. The weather condition of the day was cloudy with the maximum air temperature 24.8 ^{o}C, and minimum air temperature 13.4 ^{o}C.

Typical damage scenes are shown in **Figure 2** (**b-i**). Many buildings were collapsed or brown off their roofs, and these were covered by blue sheet (**b**). Trees were uprooted, and a wooden house was overturned upside-down with its concrete base (**e**). The Fujita scale was changed to F3 by this damage. Many objects were covered with mud because the tornado hit the area with rain (**f**). This might affect the surface temperature. Debris and mud on roads were mostly cleaned up already at the time of our field survey although some still remained. Recovery efforts were very fast because the tornado damage was localized. Restoration of electric poles and cables were going on with many trucks and workers (**i**).

3. VISIBLE AND TIR IMAGES USED AND ANALYSIS METHOD

In this study, the detection of building damage was carried out for the tornado that hit Tsukuba City. As a study area, Hojo district, a northern part of Tsukuba City, was selected where the most serious damage was observed by the tornado (**Figures 1** and **2**). Assessment of building damage was carried out using by TIR and visible images

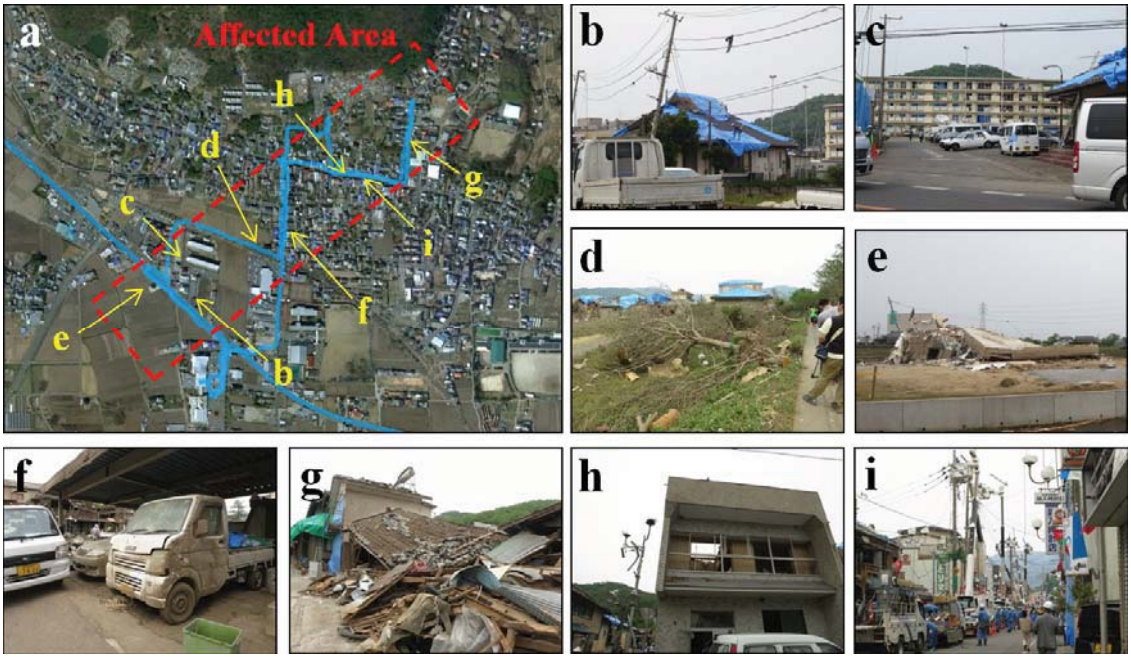

Figure 2 (a) The area of field survey in Hojo district, Tsukuba City and photo shooting locations, (b) Blue-sheet on the roof, (c) Damage on the side wall of an apartment building, (d) Fallen trees along street, (e) Overturned wooden house with its concrete base, (f) Cars stained with tornado's mud water, (g) Buildings that reduced to debris, (h) Brown-off of the roof (the sky is seen from the window), (i) Restoration work of electric poles and cables.

taken from a helicopter of SKYMAP co. by our request after the tornado. **Figure 3** (**a, c**) show a part of the post-event visible and TIR images taken at daytime (about 14:00) on May 8, 2012 while (**d**) shows a part of the TIR image taken at nighttime (about 19:30) on the day.

These images were taken from a small helicopter from the height of 460 m. The visible image with 0.25 m pixel size was created by mosaicing high-definition television (HDTV) scenes from a SONY handy video camera. The thermal-infrared (TIR) images with 1.54 m pixel size were mosaiced from ones taken by a TIR camera (NEC TS7302). Building footprints were created on a GIS system from the daytime aerial visible image by the present authors in order to use them in damage assessment for individual buildings.

The damage assessment was carried out in the following steps; Firstly building footprints were manually created from the daytime aerial visible image and an existing Zenrin digital map on ArcGIS software (**Figure 3b**). Then, damage status of each building was detected visually from the daytime aerial visible image based on the building damage classification shown in **Figure 4**. This classification was applied here, modified from the floor damage criteria by the Cabinet Office of Japan (2009), which is recommended to use when evaluating the monetary loss of residential structures for local governments. In the classification, the damage level of each wooden house is judged by 5 grades: such as no to slight (G0-G1), minor (G2), moderate (G3), major damage (G4) and collapse (G5). We employed the method based on the damaged percentage of a roof (*R*) since it is suitable to apply to vertical aerial images.

The damage level of each building was also estimated from the temperature distribution obtained from the daytime and nighttime TIR images. The average temperature and its slope angle within a building footprint were calculated and they were compared with the damage grade. The slope angle was calculated for a 3x3-pixels window (ArcGIS Resource Center, 2011). A large slope angle means a large difference in temperature between adjacent pixels while a small slope angle indicates a small difference. We considered that a severer building damage level might lead to higher variability in temperature distribution within a footprint. The average temperature within each footprint was also calculated for the daytime and nighttime TIR images using ArcGIS software. An open DXF file was generated by ArcGIS and a histogram of the average temperature for each building was made for each damage grade.

4. RESULTS OF DAMAGE EXTRACTION

4.1 Visual Damage Assessment from the Post-event Visible Image

Figure 4 shows the result of our visual damage inspection from the daytime aerial visible image. It is seen that the grades G3-G5 buildings were located along the path of the tornado. The path of the tornado was clearly seen from the visible image, and the center line was drawn as shown in **Figure 5**. The parallel lines were also drawn up to 200 m from the center line to the both sides in 20 m interval. The damage ratio for each distance class was calculated and shown also in **Figure 5**. It is observed that the collapsed

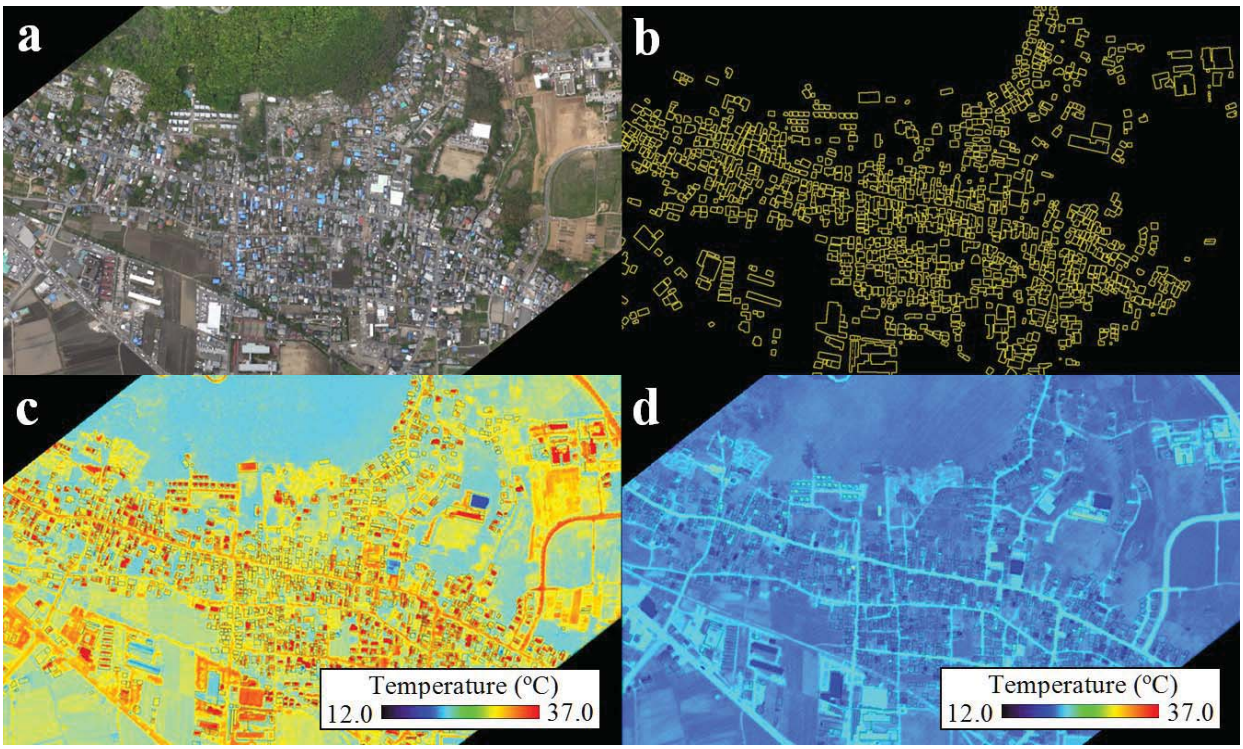

Figure 3 (**a**) Visible image of Hojo district in Tsukuba City at daytime, (**b**) building footprints created from (a), (**c**) TIR image at daytime, and (**d**) TIR image at nighttime on May 8, 2012 taken from helicopter.

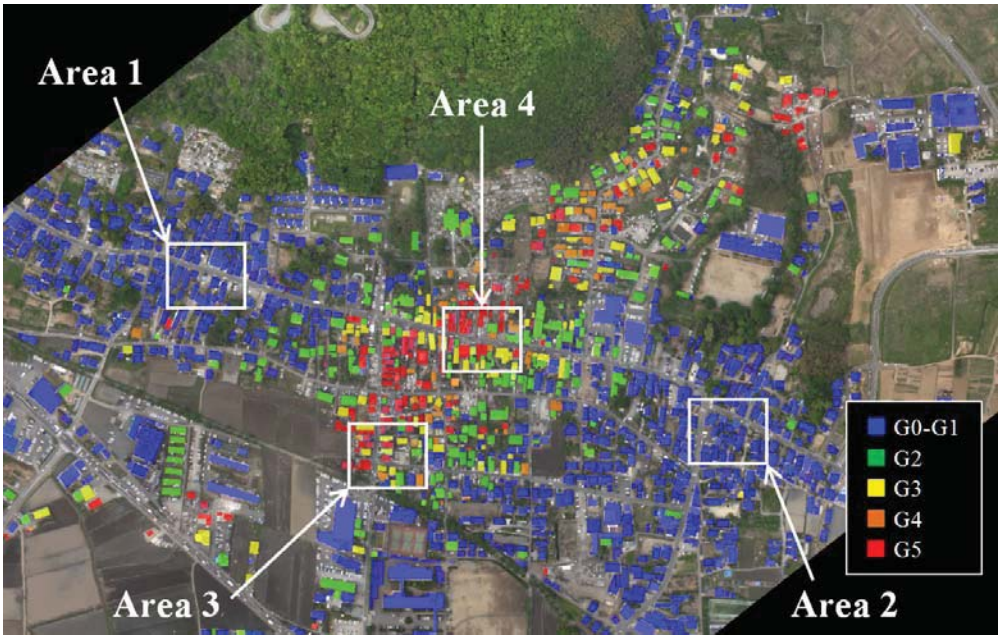

Damage Level	G2	G3	G4	G5
Roof damage ratio $R = \frac{Damaged\ Roof}{Roof}$				
	0%<R≤20%	20%≤R<50%	50%≤R<70%	R≥70%

Figure 4 Damage classification result by our visual inspection for the daytime aerial visible image.

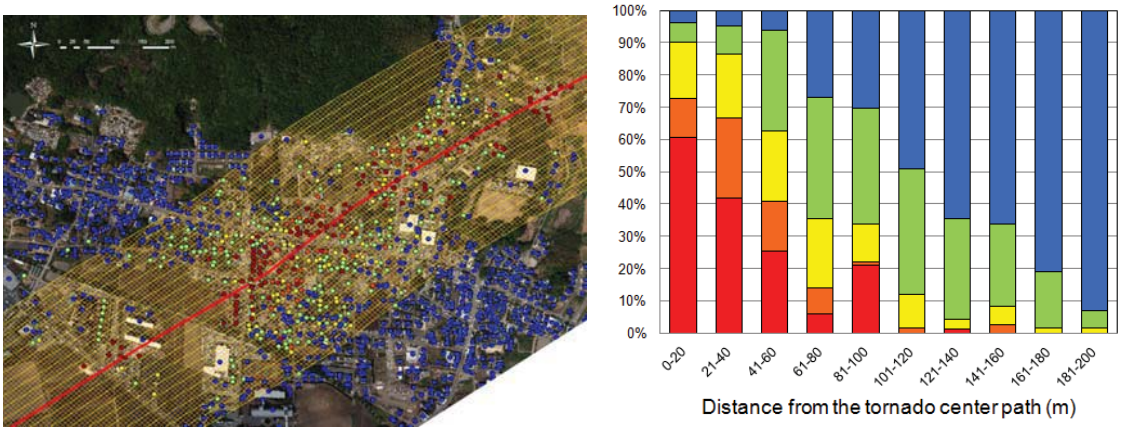

Figure 5 The center path of the tornado detected from our visual inspection and its parallel lines within 200 m (left) and the damage ratio of buildings for 20 m interval from the center path (right)

Table 2 Comparison of the result by our visual inspection on the daytime optical image and that from field observation by Tsukuba Fire Department for 730 buildings within 200 m from the tornado path in Hojo district

Visual Inspection \ Field Survey	G5	G4, G3	G2	G1, G0	User's Accuracy
G5	82	17	6	8	72.6%
G4, G3	27	56	40	22	38.6%
G2	9	34	100	39	54.9%
G1, G0	0	15	102	172	59.5%
Producer's Accuracy	69.5%	45.9%	40.3%	71.4%	Overall Acurracy 56.2%

buildings (G5) were located mostly within 60 m from the center path of the tornado. No collapsed building was found outside of the 100 m lines from the center path. Almost no damaged buildings were seen outside of the 200 m lines from the center path. The damage due to the tornado was concentrated in a narrow range although tornado paths are unpredictable.

In our visual damage inspection, some buildings were judged as no damage although some damages on their side surfaces were seen in our field survey, i.e. the apartment building in **Figure 2c**, because the damage was judged only from the roof condition of the vertical visible image. This might be the reason of the difference between our inspection result with the damage assessment result by Tsukuba Fire Department from the ground, as shown in **Table 2**. The damage assessment in their field survey was conducted by looking from outside, and thus damages to side walls and facade could mostly be seen. G3 and G4 were grouped as one class because their results did not distinguish these two.

It is seen from the table that the user's accuracy and producer's accuracy are almost the same level in this area, which indicates that both vertical photos and ground survey have weakness; the former sees only a top view while the latter mostly a side view of a building. In case of building damage due to tornados, damages to roofs prevail and hence vertical areal images are suitable to detect damages. On the contrary, damages due to earthquakes are more difficult to extract from vertical aerial images since damages to side walls are usually significant.

In this study, our visual inspection result was used as the reference data for the aerial TIR images since the both data were acquired from the same vertical view angle, where only the damage condition or the temperature of the roof was seen.

4.2 Temperature Characteristics of Non-damaged Areas from Daytime and Nighttime TIR Images

The characteristics of the TIR images at non-damaged areas were discussed first. **Figure 6** shows the locations of two target non-damaged areas in **Figure 4**. **Figure 7** shows the surface temperature within the building footprints from the daytime and nighttime TIR images, superimposed on the visible image. From the daytime roof temperature distributions in **Figure 7** (**a**, **c**), the roofs mostly show high temperature although some low temperature roofs exist. From the nighttime roof temperature distributions in **Figure 7** (**b**, **d**), the buildings showing high temperature at daytime are still in relatively higher temperature at nighttime. It is observed that the roof temperature within a footprint of a non-damaged building is mostly uniformly distributed but the effects of surrounding vegetation, shadow and footprint's inaccuracy can be observed around the outline.

Figure 8 shows the slope angle of the surface

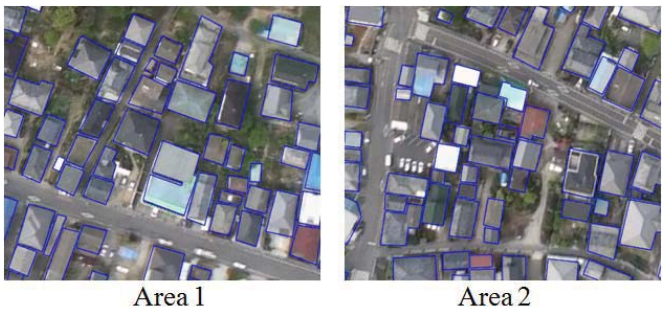

Figure 6 Target areas of non-damage in Figure 4

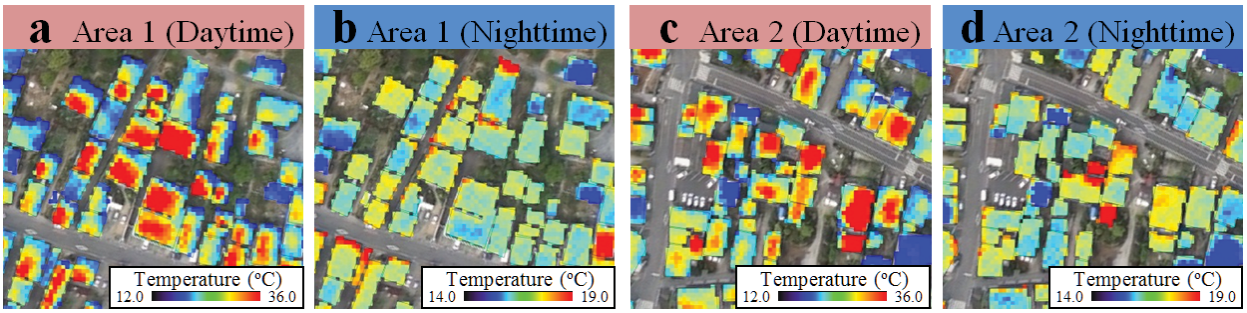

Figure 7 Temperature within building footprints for non-damage areas, **a**, **c**: Daytime, **b**, **d**: Nighttime

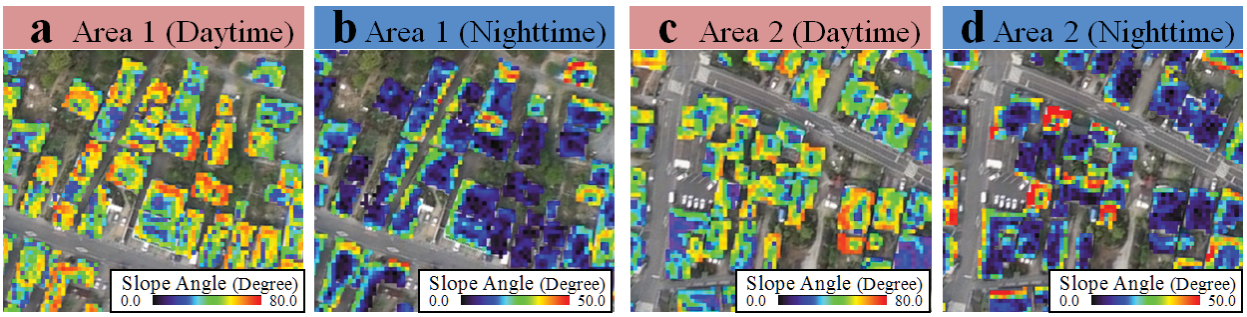

Figure 8 Slope angle of the temperature within building footprints in Figure 7, **a**, **c**: Daytime, **b**, **d**: Nighttime

temperature within the footprints. In calculation of the slope angle, the temperature of the adjacent pixels affected the result although the angle is shown only within the footprints. In the daytime slope angles in **Figures 8** (**a**, **c**), high temperature roofs show generally larger slope angles because the temperature difference with their surroundings is large due to the difference of surface materials. In the nighttime slope angles in **Figure 8** (**b**, **d**), the slope angles within some building outlines are displayed red color affected by surrounding road or vegetation. However most building roofs are in low temperature with uniform distribution, and thus their temperature changes within their outlines are small.

4.3 Temperature Characteristics of Heavily-damaged Areas from Daytime and Nighttime TIR Images

Next the characteristics of the TIR images at heavily-damaged areas were discussed. **Figure 9** show the locations of two target heavily-damaged areas in **Figure 4**. **Figure 10** shows the surface temperature within the building footprints from the daytime and nighttime TIR images, superimposed on the visible image. From the daytime roof temperature distributions in **Figure 9** (**a**, **c**), damaged roofs mostly show low temperature because they were covered by blue sheet or reduced to debris. The nighttime roof temperature distributions in **Figure 9** (**b**, **d**) also exhibit low values. The temperature distributions for heavily-damaged buildings are seen to be somewhat different from those of non-damaged ones both at daytime and nighttime, but this observation is highly affected by the material, color and orientation of the roof, shadow and surrounding conditions.

Figure 11 shows the slope angle of the surface temperature within the footprints. In the daytime slope angles in **Figure 11** (**a**, **c**), many buildings show small values as in purple to blue colors. It is also observed that the pixels with large angles are few probably because buildings were reduced debris and it spread in and outside of the original building footprints. Many materials were mixed up by building collapse and thus many objects became a

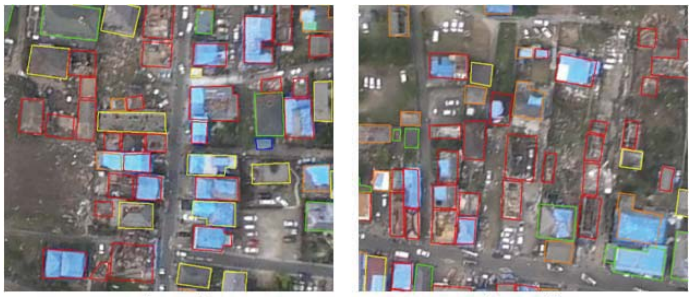

Figure 9 Target areas of heavy-damage in Figure 4

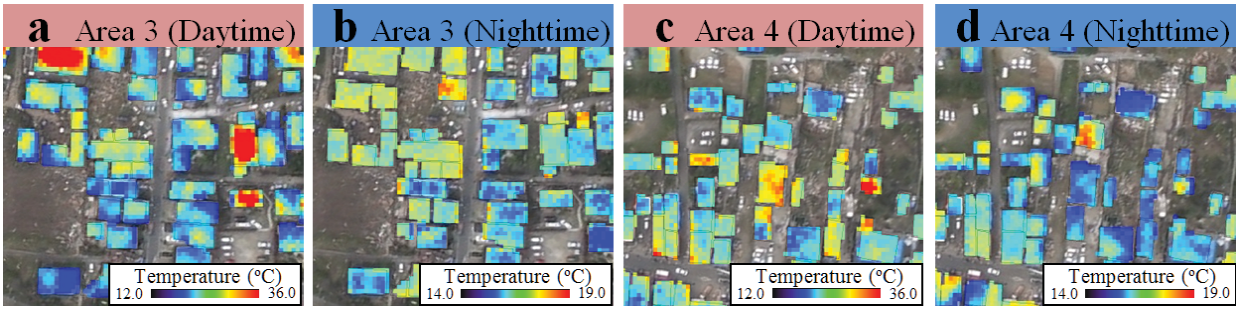

Figure 10 Temperature within building footprints for heavy-damage areas, **a**, **c**: Daytime, **b**, **d**: Nighttime

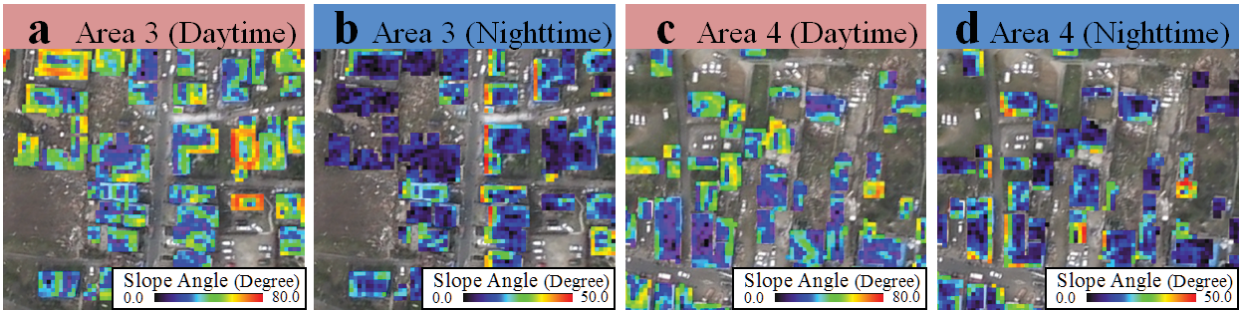

Figure 11 Slope angle of the temperature within building footprints in Figure 10, **a**, **c**: Daytime, **b**, **d**: Nighttime

mixed-pixel (mixel) condition for the low resolution TIR images (1.54 m). This characteristic is remarkable especially for the upper left building group in **Figure 11b**. Most footprint areas show small changes as in dark blue color. It can be seen in the visible image of Area 3 that the spread debris in the area became the similar condition as soil. This kind of debris spread was also observed in our field survey, and hence there is possibility to use this more uniform temperature distribution with the surroundings in early damage detection from TIR images.

4.4 Distribution of Average Temperature within Footprint for Each Damage Level

Figure 12 shows the cumulative distributions of the average temperature within building footprints for each damage level. Here, buildings other than in Hojo district were also counted. From the daytime graph, the average roof temperatures for non-damaged buildings are seen to be widely distributed in the range from 20 to 40 °C. On the contrary, those for damaged buildings are displayed in a narrower range from 24 to 35 °C and the range gets small as the damage level gets higher. For collapsed buildings (G5), the average temperature becomes in the range from 25 to 33 °C. This is because that the roofs were lost and the footprint areas were covered by the mixture of various materials like debris and mud. If we can use a much higher-resolution TIR image, a wider temperature distribution can be seen in more detail. But at this time, the resolution of our TIR images are 1.54 m, and thus most debris became in a mixel condition and the temperature distributions became flat. The histogram for damaged buildings at daytime tends to be in a narrow range and the average values were decreased for 2 or 3 °C.

From the nighttime graph, the average temperatures for most buildings are seen in narrower ranges, around 17 °C, compared with the daytime graph, as typically observed for collapsed buildings (G5). The cumulative distributions for damaged buildings at nighttime also tend to be in narrower ranges, the same as the daytime case. This kind of temperature characteristics in aerial TIR images may be used

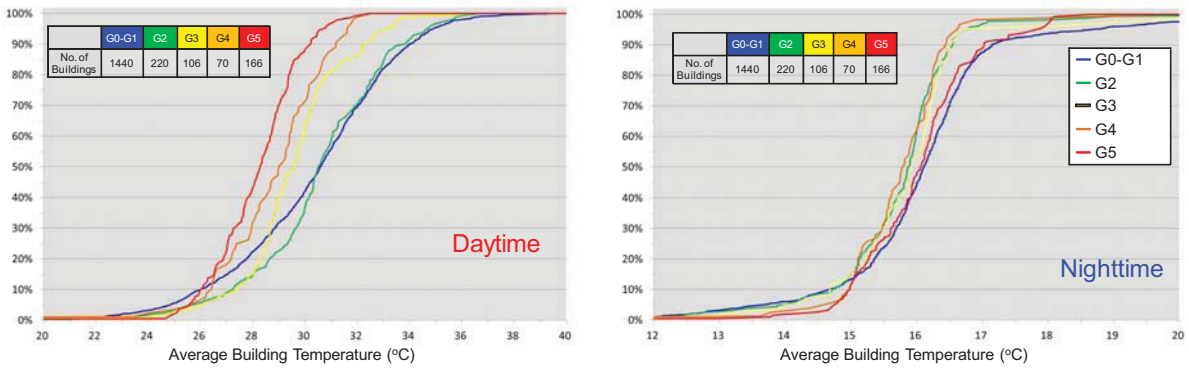

Figure 12 Cumulative distributions of average temperature within footprint for each damage level

in early damage detection in the future although more examples for various conditions should be tested.

5. CONCLUSIONS

In this study, aerial thermal infrared images were used to grasp building damages caused by the tornado that hit Tsukuba City on May 6, 2012. We acquired visible and TIR images over Hojo district of the city from a helicopter two days after the tornado struck. First building footprint data were created manually from the acquired visible image and the existing GIS map. Visual damage inspection was then carried out using the daytime visible image for the hard-hit area. The TIR images were then compared with the result of the damage inspection. The temperature distribution within the footprints was further investigated on a GIS.

From the average temperature distribution within non-damaged and damaged building footprints, non-damaged buildings showed higher temperatures with a larger range than those of damaged buildings. This observation may be explained by the fact that due to the collapse of roofs, the sunlight did not reach the roof locations and thus the temperature there was generally reduced. The change of temperature within each footprint was also evaluated using the slope angle of the temperature. But the slope angle was also strongly affected by the temperature itself, and hence a clear trend was not found.

From the distributions of the average temperature within building footprints for five damage levels, that for the collapsed level was distributed in a narrower range than that for non-damaged one's both at daytime and nighttime. The temperature distribution was seen to become flat as the damage level goes up. This is due to the mixed-pixel of debris and others around the original footprint, especially for the low spatial-resolution TIR images used in this study.

We tested the aerial TIR images after the tornado in this study because TIR imagery can be obtained even at nighttime and thus is possible to reduce "blank time" after a disaster strikes. However, due to the limitation of its spatial resolution, about 1.5 m in the current example, it was not so easy to detect small damage to individual buildings. Another important drawback of TIR imagery is that it is highly affected by the roof material, color and its orientation as well as the surrounding condition and the weather and air-temperature. Hence, more case studies are necessary in the future to utilize aerial TIR imagery for early damage detection after a disaster strike, especially at nighttime.

References:

ArcGIS resource center (2011), How Slope Works, http://help.arcgis.com/en/arcgisdesktop/10.0/help/index.html#/na/009z000000vz000000/

Cabinet Office of Japan (2009), Operational Guidelines of Damage Certification Criteria for Residences (in Japanese). URL: http://www.bousai.go.jp/hou/pdf/shishinall.pdf

Dell' Acqua, F. and Gamba, P. (2012) Remote Sensing and Earthquake Damage Assessment Experiences, Limits, and Perspectives, *Proceedings of the IEEE*, Vol. 100, No. 10, pp. 2876-2890.

Eguchi, R.T., Huyck, C., Ghosh, S., and Adams, B.J. (2008), The Application of Remote Sensing Technologies for Disaster Management, *the 14th World Conference on Earthquake Engineering*, CD-ROM.

Hanada, D., and Yamazaki, F. (2012), Detection of Flooded Areas by the Tohoku Earthquake/Tsunami Using ASTER Thermal Infrared Images, *9th International Conference on Urban Earthquake Engineering*, CD-ROM, 235-239.

Japan Meteorological Agency (2012), Report of the Tornado Occurred on May 6, 2012 (in Japanese). http://www.jma.go.jp/jma/press/1206/08b/toppu120608.html

Joyce, K.E., Belliss, S.E., Samsonov, S.V., McNeill, S.J., and Glassey, P.J. (2009), A Review of the Status of Satellite Remote Sensing and Image Processing Techniques for Mapping Natural Hazards and Disasters, *Progress in Physical Geography*, 33(2) , pp. 183–207.

Mitomi, H., Yamazaki, F., and Matsuoka, M. (2000), Automated Detection of Building Damage due to Recent Earthquakes using Aerial Television Images and Photographs, *Proc. of the 21st Asian Conference on Remote Sensing*, Vol. 1, 401-406.

Rathje, E, and Adams, B.J. (2008), The Role of Remote Sensing in Earthquake Science and Engineering, Opportunities and Challenges, *Earthquake Spectra*, 24(2), 471–492.

Tsukuba City (2012), Damage Situation by the Tornado Occurred on May 6, 2012 (in Japanese).

van Aardt, J., McKeown, D., Faulring, J., Raqueño, N., Casterline, M., Renschler, C., Eguchi, R. *et al.* (2011), Geospatial Disaster Response during the Haiti Earthquake: A Case Study Spanning Airborne Deployment, Data Collection, Transfer, Processing, and Dissemination, *Photogrammetric Engineering & Remote Sensing*, Vol. 77, No. 9, September 2011, pp. 943–952.

Yamazaki, F., Murakoshi, A., and Sekiya, N. (2009), Observation of Urban Heat Island using Airborne Thermal Sensors, *2009 Urban Remote Sensing Joint Event*, IEEE, Shanghai, China.